JOURNAL OF CATALYSIS 149, 1–10 (1994)

Thermal Stability, Acidity, Catalytic Properties, and Deactivation Behaviour of SAPO-5 Catalysts: Effect of Silicon Content, Acid Treatment, and Na Exchange

Deepak B. Akolekar

Department of Physical Chemistry, The University of New South Wales, P.O. Box 1, Kensington, NSW 2033, Australia

Received July 20, 1993; revised March 16, 1994

Crystalline microporous SAPO-5 molecular sieves with different silicon content, acid-treated SAPO-5 and Na-exchanged SAPO-5 were investigated for their thermal stability, and acidic and catalytic properties. SAPO-5 materials with increasing Si framework content exhibited lower thermal stability. The effects of the thermal treatment and Na exchange on the N_2-sorption capacity (at 78 K) of these materials were studied. *In situ* IR spectroscopic investigations of pyridine chemisorbed on the aluminophosphate catalysts revealed that the concentration of Brønsted and Lewis acid sites are strongly affected by the Si content in the $AlPO_4$ framework, acid treatment, and Na exchange. The results of temperature programmed desorption (TPD) and stepwise thermal desorption of pyridine suggest that there exists a broad site energy distribution over the aluminophosphate catalysts. The number of strong acid sites on the aluminophosphate catalysts increases with the increasing Si content in the $AlPO_4$ framework. The acid treatment and Na exchange showed a decrease in the number of strong acid sites on SAPO-5. The TPD of pyridine over SAPO-5, acid-treated SAPO-5, and Na-exchanged SAPO-5 indicated the presence of two types of acid sites. Correlation between the number of strong acid sites (measured in terms of the chemisorption of pyridine at 673 K) and framework charge on the aluminophosphate catalysts has also been obtained. The catalytic activities of SAPO-5 catalysts in the ethanol, *n*-hexane, isooctane, toluene, and *o*-xylene conversion reactions were studied. The catalytic activity of the aluminophosphate increases with the Si content in the $AlPO_4$ framework. The dependence of cumene cracking activity of the aluminophosphate on time-on-stream show that the deactivation of SAPO-5 with higher Si content is faster. A sharp increase in the deactivation rate of SAPO-5 was observed after the Na exchange.

INTRODUCTION

Crystalline microporous aluminophosphate molecular sieves were first reported by Union Carbide Corp. (1). The structural and composition variety found among the aluminophosphate molecular sieves have broadened the scope of their application (1–4). Preparations of silicon-containing aluminophosphates (SAPO-*n*) have been reported by Lok *et al.* (5). SAPO-5 (Si-containing aluminophosphates of type 5) has a three-dimensional structure with hexagonal symmetry (cell parameters $a = 1.373$ nm, $c = 0.848$ nm, and $\gamma = 120°$) and contains one-dimensional channels oriented parallel to the *c*-axis and bounded by 12-membered oxygen rings. SAPO-5 is a silicon-substituted analog of $AlPO_4$-5. $AlPO_4$-5 has neutral framework with no extraframework cations. In the silicon-containing aluminophosphates (SAPO-*n*), the incorporation of Si^{4+} in the hypothetical P^{5+} site develops a negative charge on the aluminophosphate framework and, consequently, Brønsted acidity or ion-exchange capacity is generated.

Investigations on the preparation and characterization of silicon (6–11), incorporation of silicon into the $AlPO_4$ framework (11) and catalytic properties (12, 13) have already been reported. The present investigation was undertaken in order to investigate the factors (viz. Si content in the $AlPO_4$-5 framework, acid treatment, and Na exchange) affecting the structural thermal stability, N_2 sorption capacity, acidity (Brønsted and Lewis acidity, acid strength distribution), catalytic properties, and deactivation behaviour of SAPO-5 molecular sieve.

EXPERIMENTAL

Pr_3N–$AlPO_4$-5 and Pr_3N–SAPO-5 were synthesized by the hydrothermal procedures reported earlier (4, 13). Pr_3N–$AlPO_4$-5 was obtained by hydrothermal crystallization of a gel of composition $1.5\ Pr_3N \cdot 1.0\ Al_2O_3 \cdot 1.0\ P_2O_5 \cdot 40.0\ H_2O$ at 423 K over a period of 24 h in a Teflon-coated autoclave (ca. 200 cm^3). Pr_3N–SAPO-5 materials with different Si content designated as Pr_3N–SAPO-5[A], Pr_3N–SAPO-5[B], and Pr_3N–SAPO-5[C] were obtained by crystallizing the respective gel of composition [{SAPO-5[A]: $1.5\ Pr_3N \cdot 0.044\ SiO_2 \cdot 1.0\ Al_2O_3 \cdot 0.978\ P_2O_5 \cdot 40.0\ H_2O$}, {SAPO-5[B]: $1.5\ Pr_3N \cdot 0.156\ SiO_2 \cdot 1.0\ Al_2O_3 \cdot 0.922\ P_2O_5 \cdot 40.0\ H_2O$}, {SAPO-5[C]: $1.5\ Pr_3N \cdot 0.224\ SiO_2 \cdot 1.0\ Al_2O_3 \cdot 0.898\ P_2O_5 \cdot 40.0\ H_2O$}] at 423 K for 24 h at autogenous pressure. The sources of Al_2O_3, P_2O_5, and SiO_2

0021-9517/94 $6.00

were pseudo-boehmite (Condea Chemie, FRG), orthophosphoric acid (85%, Aldrich), and Kieselgel 500 (Merck, FRG), respectively. The tri-*n*-propylamine used was synthetic grade supplied by Merck. The crystals of the aluminophosphate were washed thoroughly with deionized distilled water, filtered, and dried in an air oven at 373 K for 16 h. The organic template (tri-*n*-propylamine) was removed by calcination in the presence of air (flow rate 100 $cm^3\ min^{-1}$) at 820 K for 20 h. The acid treatment and Na exchange of SAPO-5[C] were carried out as follows: (i) SAPO-5[C] (3.0 g) was treated with hydrochloric acid solution (500 cm^3) of pH 3.7 at 318 K for 6 h; (ii) Na-exchanged SAPO-5[C2] was prepared by exchanging the calcined SAPO-5[C] (3.0 g) repeatedly with 0.2 *M* NaCl solution at 346 K for 48 h. The acid-treated SAPO-5[C1] and Na-exchanged SAPO-5[C2] were washed thoroughly with deionized water, filtered, and dried in a vacuum oven at 373 K for 12 h and calcined in the presence of air at 773 K for 6 h.

The X-ray powder diffraction data were obtained by the Holland Philips PW/1730 X-ray generator with a Ni-filtered Cu$K\alpha$ radiation source and a scintillation counter. Atomic absorption spectroscopy and gravimetric analysis were used for the elemental analysis. The N_2-sorption capacity data of the materials were obtained by N_2-dynamic adsorption/desorption technique ($p/p_0 = 0.3$) using a Quantasorb unit (Quantachrome Corp., U.S.A.). The *in situ* acidity measurements were performed on self-supported wafers (15 mg) (thickness = 10.0 mg cm^{-2}) using an infrared (IR) spectrometer (IR-580B, Perkin–Elmer, USA). The catalyst wafer was first activated *in situ* in the presence of a mixture of He and O_2 (20%) at 820 K for 5 h and further in vacuum (5×10^{-7} mbar) at 798 K for 5 h. Freshly distilled pyridine was adsorbed at 473 K for 2 h by contacting with the vapour of the liquid held at 273 K (0.12 mbar) and, subsequently, pyridine was desorbed at 473 K for 1 h under 10^{-6} mbar. To investigate Brønsted and Lewis acid site strength distribution, temperature programmed desorption (TPD) of pyridine was carried out in an ultrahigh vacuum apparatus used in the IR spectrometer. The TPD was carried out from 473 to 873 K at a linear rate of 20 K min^{-1}. Concentration of Brønsted and Lewis acid sites was determined on the basis of the absorbance of the PyB band near 1543 cm^{-1} and the PyL band near 1447 cm^{-1}, respectively. The site energy distribution of the materials was measured by the TPD of pyridine (heating rate = 5 K min^{-1}) and also by the stepwise thermal desorption (STD) of pyridine using GC techniques. The procedures for the measurement of TPD and STD of pyridine and also for evaluating the chemisorption data from the STD are reported elsewhere (14).

The catalytic activity of the catalysts in the alcohol-to-aromatics conversion, linear and branched alkanes, and aromatic hydrocarbon conversion reactions have been determined in a pulse microreactor (i.d. = 4 mm) connected to a gas chromatograph. The reaction conditions are mentioned in the respective tables and figures. Before the activity was measured, the catalyst was heated at 673 K for 1 h in a flow of helium. The details of the microreactor and the experimental procedures for measuring the catalytic activity of the catalysts were reported earlier (14). The catalytic activity and deactivation of the catalysts in the cumene cracking reaction as a function of time-on-stream were investigated by using a continuous flow microreactor. Prior to the reaction, the catalyst was activated *in situ* at 773 K for 5 h in the presence of helium (flow rate = 60 $cm^3\ min^{-1}$). Cumene reaction was carried out by passing the vapours (P_{cumene} = 8.93 mbar) along with helium (flow rate = 60 $cm^3\ min^{-1}$) over the catalyst at 673 K. The reaction products were analyzed simultaneously by on-line GC. The deactivated catalyst was regenerated at 820 K in the flow of a mixture of helium and oxygen (20%) for 5 h. In order to investigate the catalytic activity of untreated, acid-treated, and Na-exchanged SAPO-5[C, C1, C2], the methanol-to-aromatics conversion was measured as a function of time-on-stream (by using a continuous flow microreactor).

RESULTS AND DISCUSSION

The properties of $AlPO_4$-5 and SAPO-5 catalysts are presented in Table 1. The crystallinity (obtained from XRD data) and N_2-sorption capacity measurements indi-

TABLE 1

Properties of $AlPO_4$-5 and SAPO-5 Catalysts

Catalyst	Elemental composition	N_2-sorption capacity (mmol g^{-1})	Crystallinity (%)	Strong acid sites q_i (673 K) (mmol g^{-1})
$AlPO_4$-5	$(0.50Al \cdot 0.50P)\ O_2$	4.90	100	0.0025
SAPO-5[A]	$(0.011Si \cdot 0.500Al \cdot 0.489P)\ O_2$	4.86	100	0.0033
SAPO-5[B]	$(0.036Si \cdot 0.501Al \cdot 0.464P)\ O_2$	4.84	100	0.0053
SAPO-5[C]	$(0.083Si \cdot 0.501Al \cdot 0.416P)\ O_2$	4.87	100	0.0112
SAPO-5[C1] (Acid-treated)	$(0.056Si \cdot 0.502Al \cdot 0.444P)\ O_2$	4.28	93	0.0081
Na–SAPO-5[C2] (Na-exchanged)	$0.065Na\ (0.082Si \cdot 0.500Al \cdot 0.417P)\ O_2$	1.81	100	0.0015

TABLE 2

Changes in the Crystallinity and N_2-sorption Capacity of $AlPO_4$-5 and SAPO-5 Catalysts with the Calcination Temperature

Catalyst	Crystallinity (as $AlPO_4$-5) (%)				N_2-sorption capacity (mmol g^{-1})		
	820 K	918 K	973 K	1273 K	820 K	973 K	1273 K
$AlPO_4$-5	100	98	86	83	4.90	4.62	4.22
SAPO-5[A]	100	97	85.1	80	4.86	4.58	4.20
SAPO-5[B]	100	94	82.1	76.5	4.84	4.50	4.10
SAPO-5[C]	100	90	76.1	70.2	4.87	4.36	4.00
SAPO-5[C1]	93	85	74.0	69.8	4.28	4.10	3.90

cated the highly crystalline nature of the catalysts. The observed decrease in the crystallinity and N_2-sorption capacity of the acid-treated SAPO-5[C1] is due to its lower structural stability in the acidic media. In our earlier investigation (15), it was observed that the structure and other properties of $AlPO_4$-5 are very sensitive to acid–base treatments. After the sodium exchange, the pore openings and inner channels of SAPO-5[C] are partially blocked by Na^+ cations. Hence the difference between the N_2-sorption capacities of SAPO-5[C] and Na-exchanged SAPO-5[C2] is large.

The results of changes in the crystallinity and N_2-sorption capacity of $AlPO_4$-5 and SAPO-5 catalysts with the calcination temperature are presented in Table 2. $AlPO_4$-5 shows the highest thermal stability. The crystallinity and N_2-sorption capacity of SAPO-5 catalysts decrease with the calcination temperature. The acid-treated SAPO-5[C1] showed the lowest thermal stability and N_2-sorption capacity. The results lead to the conclusion that the structural stability (above the calcination temperature of 918 K) decreases with the increasing silicon content in the $AlPO_4$-5 framework. These results are consistent with those of MAPO-43 (16) and MAPO-46 (17), both containing a high concentration of framework substituted magnesium [MAPO-43: Mg 11.2 mol%; MAPO-46: Mg 9.9 mol%)]. The crystal structure of MAPO-43 and MAPO-46 are thermally stable up to 698 and 753 K, respectively.

Figure 1 shows the hydroxyl region of the infrared spectra of SAPO-5 catalysts after vacuum activation at 798 K. The band at 3735 cm^{-1} is characteristic of terminal OH or impurities, while the bands at 3665 and 3629 cm^{-1} are assigned to the lattice terminating P–OH group and acidic hydroxyl group (18–20), respectively. The incorporation of Si into the aluminophosphate framework generates the acidic hydroxyls. These acidic hydroxyls are generated after the removal of organic template at 798 K. The anionic framework charge generated by the Si substitution leads to Brønsted acidity. IR spectra show that the number of skeletal bridging hydroxyls (–Si–OH–Al–) varies with the number of skeletal Si. The concentration of acidic hydroxyl is higher over SAPO-5[C] than in the $AlPO_4$-5 and SAPO-5[A,B,C1,C2] materials. The partial dissolution of the silico–aluminophosphate during the acid treatment affects the concentration of acidic hydroxyls; this is observed in the case of acid treated SAPO-5[C1]. Also it is interesting to note that in the case of Na-exchanged SAPO-5[C2], the external protons [P–OH, 3665 cm^{-1}] were almost replaced by Na cations, while the protons in the channels (Si–OH–Al, 3629 cm^{-1}] were only partially exchanged by Na cations.

The results of the absorbance (at 1447 and 1543 cm^{-1} bands) of pyridine adsorbed at 473 K on the catalysts (Fig. 2A) indicated the highest concentration of Lewis acid sites over $AlPO_4$-5 and the highest concentration of Brønsted acid sites over SAPO-5[C]. The higher absorbance of pyridine (at 1447 cm^{-1}, Lewis acid sites) on

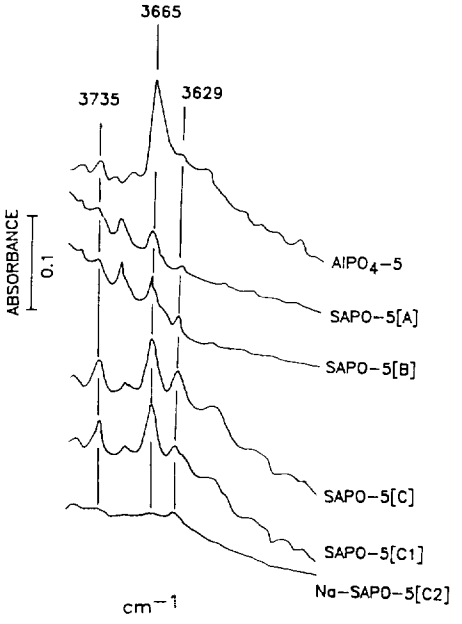

FIG. 1. Hydroxyl region of the infrared spectra of $AlPO_4$-5, SAPO-5[A–C], acid-treated SAPO-5[C1], and Na-exchanged SAPO-5[C2] after vacuum activation at 798 K.

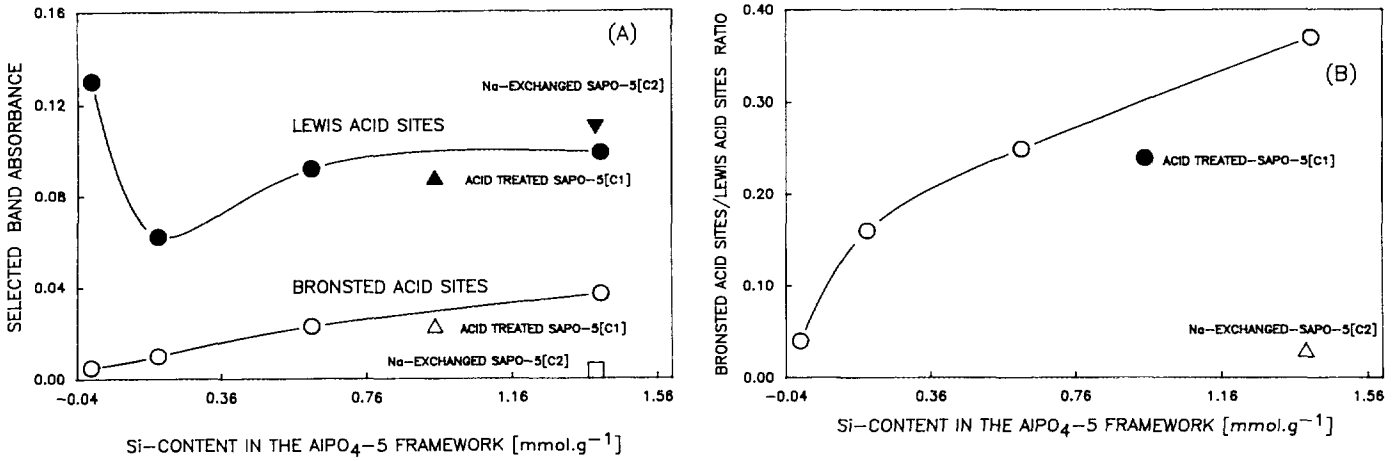

FIG. 2. Changes in (A) Brønsted and Lewis acid site density and (B) the ratio of the absorbance of the bands at 1543 cm^{-1} (Brønsted acid sites) and 1447 cm^{-1} (Lewis acid sites) of the pyridine adsorbed at 473 K over the aluminophosphate catalysts containing varying amount of silicon, acid-treated SAPO-5[C1], and Na-exchanged SAPO-5[C2].

Na-exchanged SAPO-5[C2] compared with that of SAPO-5[C] is due to the interaction between Na^+ cations and pyridine molecules. It is observed that Brønsted acidity increases with the increase of Si in the aluminophosphate framework. Brønsted acidity is affected by the acid treatment and Na exchange of SAPO-5[C]. The order of the concentration of Brønsted acid sites over the catalysts is as follows: SAPO-5[C] > acid-treated SAPO-5[C1] > SAPO-5[B] > SAPO-5[A] > AlPO-5 > Na-exchanged SAPO-5[C2]. Figure 2B shows the variation in Brønsted to Lewis acid sites ratio with the Si content in the $AlPO_4$-framework, acid-treated SAPO-5[C1], and Na-exchanged SAPO-5[C2] at 473 K. The ratio of Brønsted to Lewis acid sites increases with the increase of Si content in the $AlPO_4$ framework. The results of the changes in the absorbance [(1543 cm^{-1}, Fig. 3A) (1447 cm^{-1}, Fig. 3B)] of pyridine as a function of evacuation temperature indicated that Lewis and Brønsted acid sites of different energies exist on $AlPO_4$-5 and SAPO-5 materials. On all the catalysts, the concentration of Lewis acid sites is higher than that of Brønsted acid sites. With the increase in the evacuation temperature a decrease in the concentration of Brønsted and Lewis acid sites is observed. Moffat *et al.* (21) applied the semiempirical CNDO/2 quantum chemical calculation on a cluster model of $ALPO_4$-5 and found that the oxygen atoms possess negative charge and function as Lewis base sites. Phosphorous atoms with higher positive charge as compared with aluminium atoms act as Lewis acid sites, and Brønsted acid sites are the protons attached to terminal oxygen atoms on the surface of aluminophosphate. Therefore, there are very few Brønsted acid sites and the majority of acid sites are Lewis acid sites in the $AlPO_4$ molecular sieves. Also lattice imperfections are probably the source of the weak acid sites.

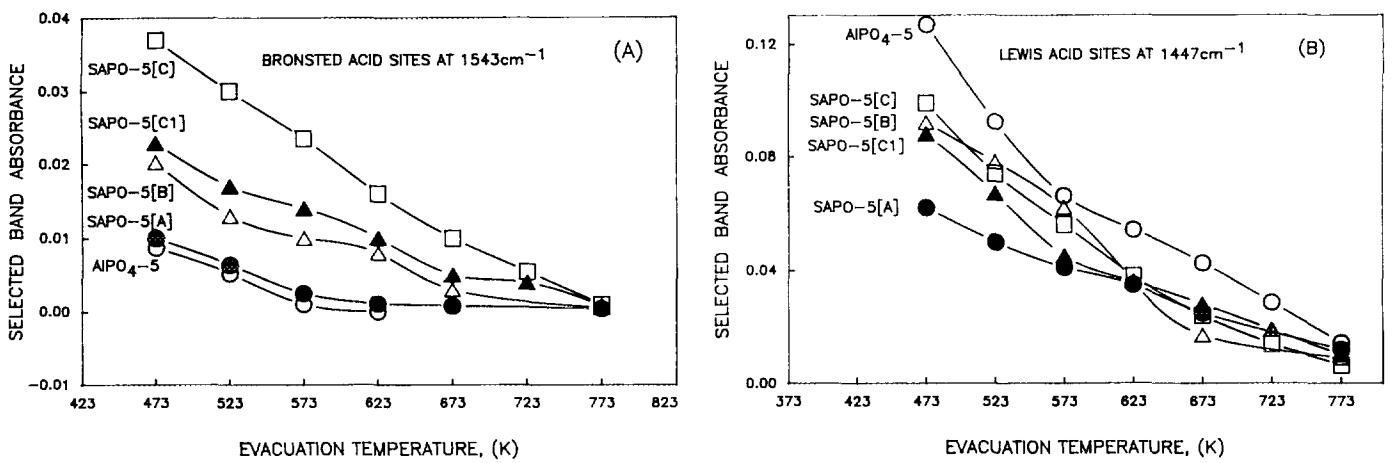

FIG. 3. Changes in the absorbance of pyridine band (A) at 1543 cm^{-1} (Brønsted acid sites) and (B) at 1447 cm^{-1} (Lewis acid sites) for $AlPO_4$-5 and SAPO-5 catalysts as a function of evacuation temperature.

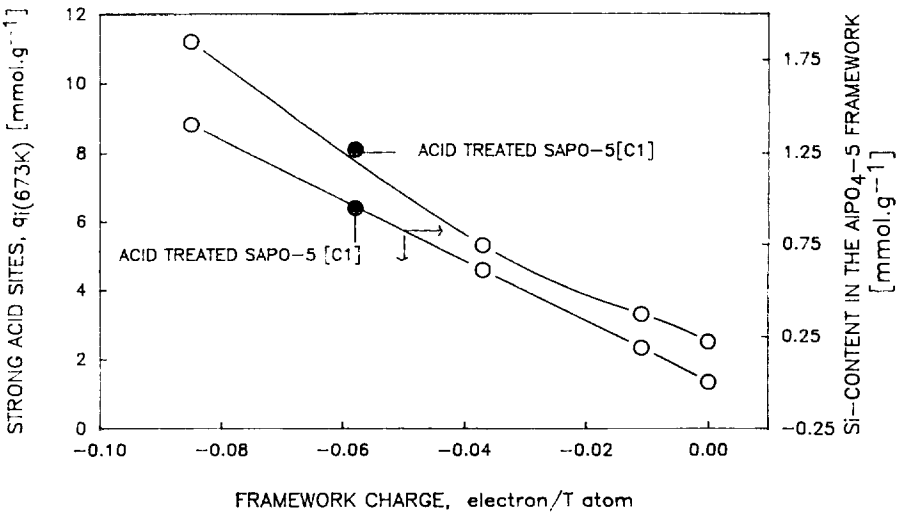

FIG. 4. Correlation between the strong acid sites and the framework charge on $AlPO_4$-5 and SAPO-5 catalysts.

Correlation between the acidity (strong acid sites measured in terms of the amount of pyridine chemisorbed at 673 K) and the framework charge (obtained from the elemental composition) of the catalysts is presented in Fig. 4. From the correlation, it is concluded that the number of strong acid sites is increased with the decrease in the framework charge on the aluminophosphate-based catalysts. The TPD chromatograms of pyridine on SAPO-5 catalysts at the heating rate of 5 K min^{-1} are shown in Fig. 5. In the TPD chromatograms, two peaks are observed, which indicates the involvement of two types of active site in the desorption process. The desorption appears to be first order as the chromatograms are asymmetric. The values of the maximum temperature (T_m) for the two peaks are given below:

	SAPO-5[C]	Acid-treated SAPO-5[C1]	Na-exchanged SAPO-5[C2]
First peak T_m (K)	573	531	492
Second peak T_m (K)	673	673	673

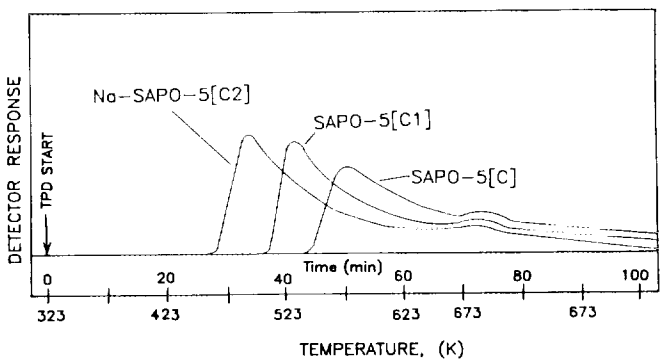

FIG. 5. TPD chromatograms of pyridine on SAPO-5[C], acid-treated SAPO-5[C1], and Na-exchanged SAPO-5[C2] (amount of catalyst = 0.20 g; He-flow rate = 10 cm^3 min^{-1}; heating rate = 5 K min^{-1}; pyridine injected = 2.0 μl).

Comparisons of the TPD chromatograms (Fig. 5) show that the strength distribution of the pyridine adsorption sites of SAPO-5[C] is significantly affected by the acid treatment and Na exchange. In the case of acid-treated SAPO-5[C1], the peak maximum temperature of the first peak is lower than that observed for untreated SAPO-5[C]. This is attributed to the partial destruction of some of the acid sites during the acid treatment of SAPO-5[C], which also affects its catalytic properties. The peak maximum temperature for the first peak of Na-exchanged SAPO-5[C2] is shifted towards the lower energy region.

Figure 6 shows the temperature dependence of the chemisorption of pyridine on the aluminophosphate catalysts. The chemisorption data were obtained from the STD data by the procedure described earlier (14). The chemisorption of pyridine at higher temperatures points to the involvement of the stronger sites. The q_i vs T curve, therefore, presents a type of site energy distribution in which

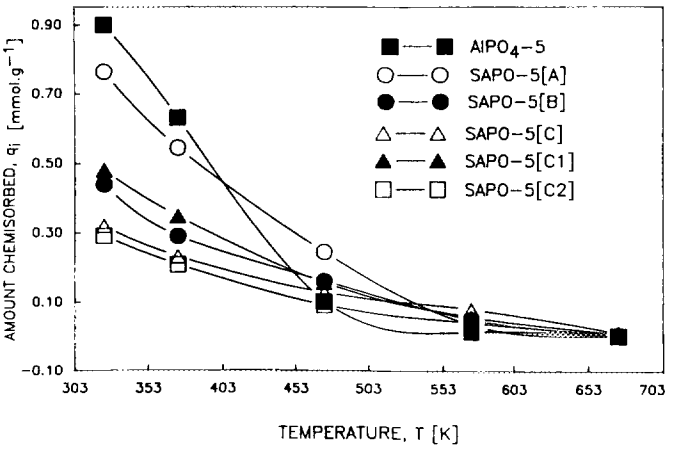

FIG. 6. Temperature dependence of the chemisorption of pyridine on $AlPO_4$-5 and SAPO-5 catalysts.

the number of sites is expressed in terms of the amount of pyridine chemisorbed as a function of the sorption temperature. The site energy distribution obtained from the STD of pyridine on the aluminophosphate catalysts is shown in Fig. 7. The strength of the site involved in the pyridine chemisorption is expressed in terms of the desorption temperature (T_d), which lies in the range of temperatures in which the chemisorbed pyridine is desorbed. Here, T_d^* is the temperature at which the pyridine chemisorbed on the strongest sites was desorbed. The columns in Fig. 7 show the strength distribution of the sites involved in the chemisorption at the lowest temperature of the STD (i.e., 323 K). The sites of strength 673 K $< T_d \leq T_d^*$ were obtained from the amount of pyridine chemisorbed at 673 K. On the other hand, the sites of strength $T_1 < T_d \leq T_2$ were obtained from the amount of pyridine which was initially chemisorbed at T_1 but desorbed by increasing the temperature to T_2. The results (Figs. 6 and 7) indicate that the site energy distribution and the number of strong acid sites (measured in terms of the chemisorption of pyridine at 673 K) on the aluminophosphate catalysts are strongly influenced by the Si content in the aluminophosphate framework and acid treatment. The degree of Na^+ exchange also affects the site energy distribution; however, its influence is pronounced, particularly on the high energy sites. The order of the strong acid sites over the aluminophosphates is as follows: SAPO-5[C] > acid treated SAPO-5[C1] > SAPO-5[B] > SAPO-5[A] > $AlPO_4$-5 ≥ Na-exchanged SAPO-5[C2].

In Table 3, the results of ethanol conversion over the aluminophosphate catalysts are compared. In ethanol conversion reaction, SAPO-5[C] showed the highest conversion and concentration of aromatics formed. The highest conversion is attributed to the presence of more strong acid sites on SAPO-5[C]. The observed order of catalytic activity and aromatics selectivity is the same as the order found for strong acid sites. Concurrent investigations on the acidity and acid strength distribution on these materials indicated that the concentration of Brønsted acid sites is the highest on SAPO-5[C]. Also the temperature programmed desorption and stepwise thermal desorption of pyridine over these materials showed that the amount of pyridine chemisorbed on SAPO-5[C] above 673 K was the highest, indicating the presence of the strongest acidic sites. The observed conversion changes are accompanied by parallel changes in the product distribution, a higher activity yielding more aromatics and less C_1 to C_5 aliphatics. The aliphatics distribution results show that the formation of C_2 aliphatics decreases and the formation of C_{3+} aliphatics increases with the acidity of the aluminophosphate catalysts. The different distribution of the aromatics is found on the different catalysts. SAPO-5[C] shows higher xylene formation and lower toluene and C_{9+} aromatics formation. The formation of C_{9+} aromatics in the ethanol conversion is the highest on $AlPO_4$-5. In the case of Na-exchanged SAPO-5[C2], the results show a strong influence of the Na^+ exchange on the catalytic activity and aromatic selectivity in the ethanol conversion reaction.

The influence of Si content in the $AlPO_4$ framework, acid treatment, and Na exchange on the catalytic activity and aromatic selectivity of the aluminophosphate catalysts in the *n*-hexane and isooctane conversion reactions is presented in Figs. 8A and 8B. The catalytic activity and aromatic selectivity increases with the Si content in the $AlPO_4$ framework. The results of the acid-treated SAPO-5[C1] show that the catalytic activity and aromatic selectivity in these reactions are affected by the acid treatment. After the sodium exchange of the SAPO-5[C], the acidity of the material decreases, which in turn affects the catalytic activity. This is reflected in the decreased catalytic activity of Na-exchanged SAPO-5[C2] in *n*-hex-

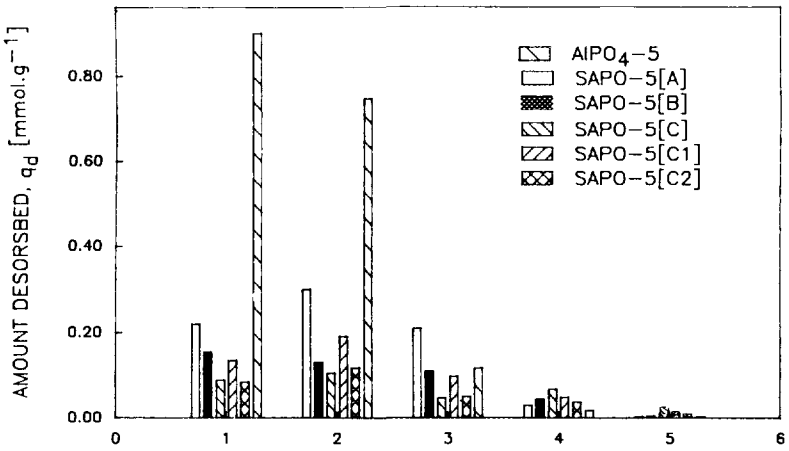

FIG. 7. Acid strength distribution of $AlPO_4$-5 and SAPO-5 catalysts. (1) 323 K < T_d < 373 K; (2) 373 K < T_d < 473 K; (3) 473 K < T_d < 573 K; (4) 573 K < T_d < 673 K; (5) 673 K < T_d < T_d^*.

TABLE 3

Conversion of Ethanol over $AlPO_4$-5 and SAPO-5 Catalysts at 673 K

Catalyst	$AlPO_4$-5	SAPO-5[A]	SAPO-5[B]	SAPO-5[C]	SAPO-5[C1]	SAPO-5[C2]
Conversion (%)	40.0	49.0	53.0	78.0	65.0	23.1
Aromatics concentration (wt%)	1.8	2.6	2.9	5.8	3.7	0.3
			Product distribution (wt%)			
CH_4	—	—	—	0.1	0.1	—
C_2 Aliphatics	97.8	93.6	93.1	90.6	92.4	98.2
C_3 Aliphatics	0.3	0.4	0.6	1.2	0.8	0.2
C_4 Aliphatics	0.3	0.4	0.5	0.8	0.7	0.1
C_{5+} Aliphatics	0.2	0.3	0.3	0.5	0.4	0.2
Aromatics	4.5	5.3	5.5	7.4	5.7	1.3
Total	100	100	100	100	100	100
			Aromatics distribution (wt%)			
Benzene	3.4	3.5	3.1	3.3	2.6	
Toluene	5.1	4.9	6.0	4.4	5.4	
Ethylbenzene	2.0	2.2	1.2	3.0	2.1	
Xylenes	48.8	51.2	53.0	61.6	56.5	
C_{9+} Aromatics	40.7	38.2	36.7	30.7	33.7	
Total	100	100	100	100	100	

Note. Reaction conditions: amount of catalyst = 0.200 g; He flow rate = 40 cm^3 min^{-1}; pulse size = 2 μl.

ane and isooctane conversion reactions. Also the presence of Na^+ cations in the channels causes a small but significant decrease in the effective channel diameter of SAPO-5. So the penetration/diffusion of large molecules such as isooctane is relatively difficult or slow. In the case of Na-exchanged SAPO-5[C2], the conversion of isooctane is drastically reduced.

The dependence of cumene cracking activity of $AlPO_4$-5 and SAPO-5 catalysts on time-on-stream is shown in Fig. 9. SAPO-5[C] shows higher cumene cracking activity than the other catalysts, which is due to the presence of stronger acid sites. A comparison of the results shows that the overall decrease in cumene cracking activity of SAPO-5[C] with time-on-stream is much steeper than with the other catalysts. Because of the higher acidity, the SAPO-5[C] deactivates faster. Cumene conversion and formation of carbonaceous products (coke) increases with the acidity. The slow deactivation of $AlPO_4$-5 is attributed to its weak acidity and lower catalytic activity (14, 22). The influence of time-on-stream on the fractional cumene cracking activity (x) [where x = (conversion of cumene at a particular period)/(initial conversion of cumene)] of $AlPO_4$-5 and SAPO-5 catalysts shown in Fig. 10 represents the deactivation trends. The higher deactivation rate of

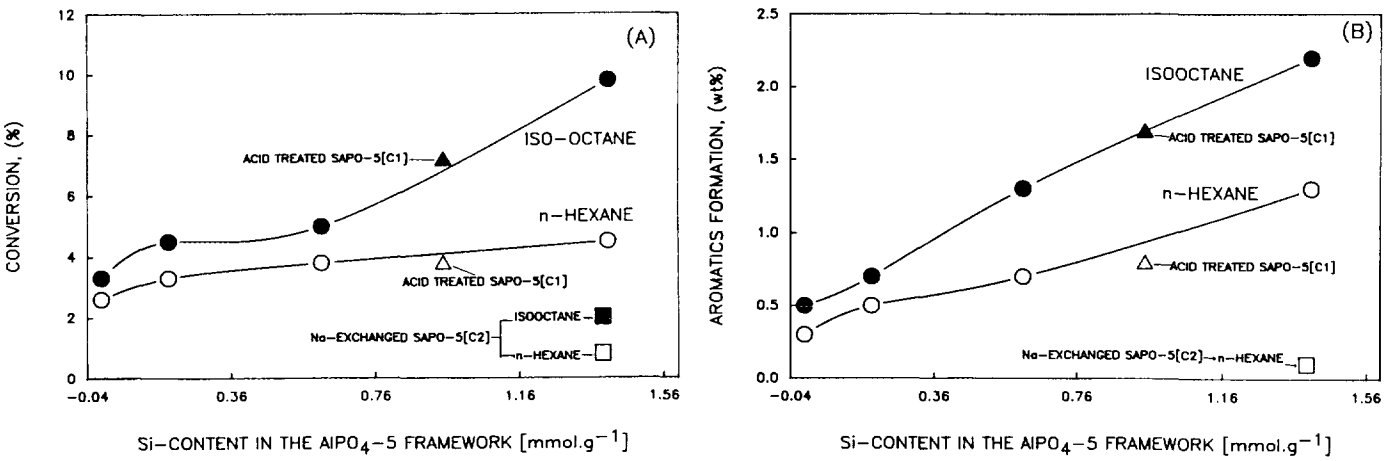

FIG. 8. (A) Variation in the conversion of isooctane and *n*-hexane over $AlPO_4$-5, SAPO-5[A–C], acid-treated SAPO-5[C1], and Na-exchanged SAPO-5[C2] (reaction conditions: amount of catalyst = 0.30 g; He flow rate = 20 cm^3 min^{-1}; temperature = 673 K; pulse size = 1 μl). (B) Formation of aromatics in the conversion of isooctane and *n*-hexane over $AlPO_4$-5, SAPO-5[A–C], acid-treated SAPO-5[C1], and Na-exchanged SAPO-5[C2].

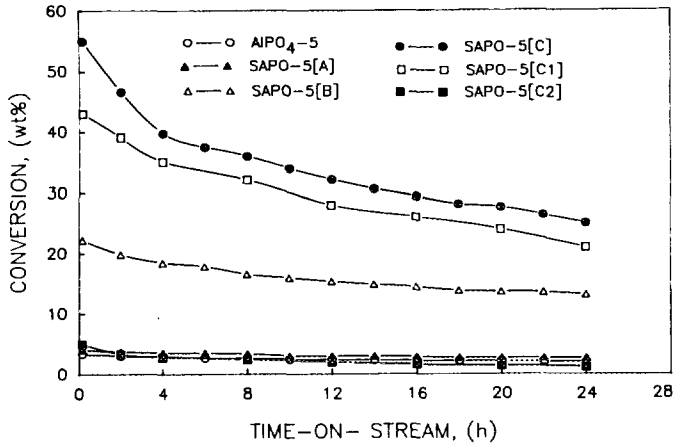

FIG. 9. Catalytic activity of $AlPO_4$-5, SAPO-5[A–C], acid-treated SAPO-5[C1], and Na-exchanged SAPO-5[C2] in cracking of cumene as a function of time-on-stream.

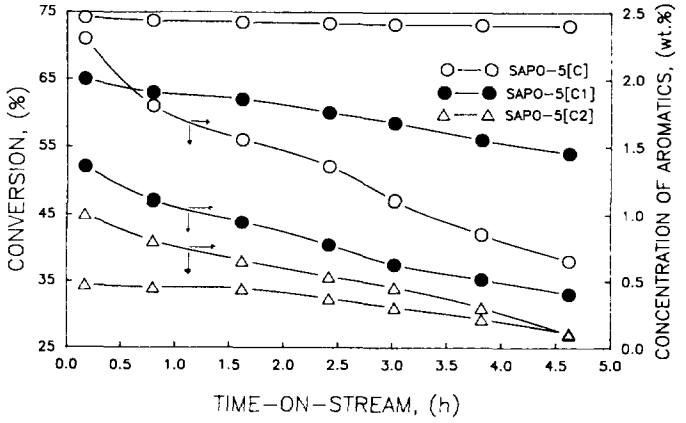

FIG. 11. Conversion and concentration of aromatics in the methanol reaction over SAPO-5[C], acid-treated SAPO-5[C1], and Na-exchanged SAPO-5[C2] as a function of time-on-stream (reaction conditions: amount of catalyst = 0.20 g; He flow rate = 45 cm^3 min^{-1}; temperature = 673 K; temperature of methanol saturator = 288 K).

Na-exchanged SAPO-5[C2] is due to the presence of Na^+ cation in the channels of SAPO-5, which reduces the effective pore diameter and, consequently, diffusion out of large aromatic hydrocarbons is drastically affected. The deactivation of $AlPO_4$-5 and SAPO-5 catalysts (by coking) depends on their acidity and, consequently, on the factors (viz. Si content, Na exchange, acid treatment, poisoning, etc.) affecting these properties. The regeneration of the deactivated $AlPO_4$-5 and SAPO-5 catalysts (at elevated temperature [825 K] and in the presence of helium and oxygen [20%] mixture) showed their cumene cracking activity to be recovered to a large extent (92–95%). The large recovery in the catalytic activity reveals that the deactivation is caused by blockage of the channels by sorbed or occluded large hydrocarbon molecules. The remaining loss (5–8%) in the catalytic activity of the regenerated catalysts is due to the deactivation of some of the strong acid sites by strongly sorbed carbonaceous species.

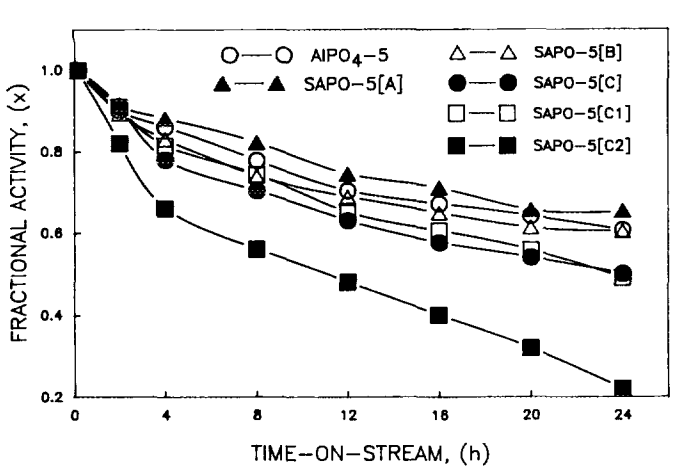

FIG. 10. Changes in the fractional catalytic activity of $AlPO_4$-5, SAPO-5[A–C], acid-treated SAPO-5[C1] and Na-exchanged SAPO-5[C2] in cracking of cumene with time-on-stream.

The untreated, acid treated, and Na-exchanged SAPO-5 catalysts are compared for their catalytic activity and aromatic selectivity in the methanol conversion reaction as a function of time-on-stream (Fig. 11). SAPO-5[C] shows higher catalytic activity and aromatics formation than acid-treated and Na-exchanged catalysts. The decreased acidity of the SAPO-5[C] after the acid treatment and Na exchange lowers the formation of aromatics.

The product distribution in toluene disproportionation on $AlPO_4$-5 and SAPO-5 catalysts at 673 K is given in Table 4. The results of toluene disproportionation indicated that the conversion of toluene increases with the number of strong acid sites over the aluminophosphates (i.e., with the increase in the Si content in the aluminophosphates). The acid treatment and the Na exchange affects the toluene disproportionation activity of SAPO-5 catalysts. SAPO-5[C] showed higher catalytic activity in *o*-xylene isomerization (Table 5) and formation of more benzene and toluene. Also the xylene loss is the highest for SAPO-5[C]. The observed order of catalytic activity (in toluene disproportionation and *o*-xylene isomerization) is the same as the order found for strong acid site concentrations, namely, SAPO-5[C] > acid-treated SAPO-5[C1] > SAPO-5[B] > SAPO-5[A] > $AlPO_4$-5 > Na-exchanged SAPO-5[C2]. In the case of Na-exchanged SAPO-5[C2], the observed increase in *p*-X/*m*-X ratio in the toluene disproportionation and *o*-xylene isomerization is a result of the diffusion–reaction interaction. The presence of Na^+ in the channels increases the diffusional resistance. The effective channel diameter is reduced as H^+ (with negligibly small ionic diameter) is replaced by Na^+ (ionic diameter 0.19 nm).

TABLE 4

Product Distribution in the Disproportionation of Toluene in $AlPO_4$-5 and SAPO-5 Catalysts at 673 K

Catalyst	$AlPO_4$-5	SAPO-5[A]	SAPO-5[B]	SAPO-5[C]	SAPO-5[C1]	SAPO-5[C2]
Conversion (%)	1.8	3.6	6.7	10.6	7.4	1.1
			Product distribution [hydrocarbon (wt%)]			
Aliphatics	0.1	0.1	0.1	0.2	0.1	—
Benzene	0.3	0.6	1.4	3.9	1.6	0.1
Toluene	98.2	96.4	93.3	89.4	92.6	98.9
p-Xylene	0.2	0.4	0.8	1.2	0.9	0.3
m-Xylene	0.3	0.6	1.1	1.5	1.2	0.3
o-Xylene	0.3	0.7	1.4	1.8	1.4	0.4
C_{9+} Aromatics	0.6	1.1	1.9	2.0	2.4	—
Total	100	100	100	100	100	100
p-X/*m*-X	0.67	0.67	0.73	0.80	0.75	1.0
p-X/*o*-X	0.67	0.57	0.57	0.67	0.64	0.75

Note. Reaction conditions: amount of catalyst = 0.300 g; He flow rate = 40 cm^3 min^{-1}; pulse size = 2 μl.

TABLE 5

Isomerization of *o*-Xylene over $AlPO_4$-5 and SAPO-5 Catalysts at 673 K

Catalyst	$AlPO_4$-5	SAPO-5[A]	SAPO-5[B]	SAPO-5[C]	SAPO-5[C1]	SAPO-5[C2]
Conversion (%)	16.2	25.0	32.9	49.4	42.3	5.6
			Product distribution [hydrocarbon (wt%)]			
Aliphatics	—	0.1	0.2	0.4	0.4	—
Benzene	0.4	0.4	0.5	0.6	0.5	0.2
Toluene	0.8	1.2	1.9	3.4	2.4	0.4
p-Xylene	5.0	9.5	12.4	17.7	16.0	2.2
m-Xylene	6.4	11.0	15.0	24.2	20.0	2.4
o-Xylene	84.8	75.0	67.1	50.6	57.7	94.4
C_{9+} aromatics	2.6	2.8	2.9	2.7	3.0	0.4
Total	100	100	100	100	100	100
p-X/*m*-X	0.78	0.83	0.83	0.73	0.80	0.92
Xylene loss (wt%)	3.8	4.5	5.5	7.5	6.3	1.0

Note. Reaction conditions: amount of catalyst = 0.200 g; He flow rate = 30 cm^3 min^{-1}; pulse size = 1 μl.

CONCLUSIONS

The thermal stability (at 820 K) of the aluminophosphate of type 5 catalysts decreases with the framework Si content and acid treatment. The crystallinity and N_2-sorption capacity of these materials decrease with the calcination temperature. The N_2-sorption capacity of SAPO-5[C] is affected by the acid treatment and Na exchange. The concentration of acidic hydroxyls increases with the Si content in the $AlPO_4$ framework. The Si content in the $AlPO_4$ framework, acid treatment, and Na exchange shows a strong influence on the acidity (concentration of Brønsted and Lewis acid sites, Brønsted to Lewis acid sites ratio, site energy distribution and strong acid sites) of the aluminophosphate of type 5 catalysts. The catalytic properties and deactivation of the aluminophosphate of type 5 catalysts are significantly affected by the Si content in the $AlPO_4$ framework, acid treatment, and Na exchange.

ACKNOWLEDGMENTS

The author is sincerely thankful to Dr. H. G. Karge, Fritz Haber Institute of the Max Planck Society, Berlin, Germany for providing the experimental facilities and helpful discussions. The author is grateful to the Alexander von Humboldt Foundation, Bonn, Germany for an award of an international research fellowship.

REFERENCES

1. Flanigen, E. M., Lok, B. M., Patton, R. L., and Wilson, S. T., *in* "Proceedings of 7th International Zeolite Conference," p. 103. Kodansha/Elsevier, Tokyo/Amsterdam, 1986.

2. Wilson, S. T., and Flanigen, E. M., *ACC Symp. Ser.* **398,** 329 (1989).
3. Flanigen, E. M., Patton, R. L., and Wilson, S. T., *Stud. Surf. Sci. Catal.* **37,** 13 (1988).
4. Wilson, S. T., Lok, B. M., Messina, C. A., and Flanigen, E. M., *ACS Symp. Ser.* **218,** 79 (1983).
5. Lok, B. M., Messina, C. A., Patton, R. L., Gajek, R. T., Cannan, T. R., and Flanigen, E. M., *J. Am. Chem. Soc.* **104,** 1146 (1982).
6. Mertens, M., Martens, J. A., Grobet, P. J., and Jacobs, P. A., *in* "Guidelines for Mastering the Properties of Molecular Sieves" (D. Barthomeuf *et al.*, Eds.), p. 1. NATO ASI Series B: Physics, Vol. 221, Plenum, New York, 1990.
7. Tapp, N. J., Milestone, N. B., and Bibby, D. M., *Stud. Surf. Sci. Catal.* **37,** 393 (1988).
8. Martens, J. A., Mertens, M., Grobet, P. J., and Jacobs, P. A., *in* "Guidelines for Mastering the Properties of Molecular Sieves" (D. Barthomeuf *et al.*, Eds.), p. 97. Nato ASI Series B: Physics, Vol. 221, Plenum, New York.
9. Freude, D., Ernst, H., Hunger, M., Pfeifer, H., and Jahn, E., *Phys. Chem. Lett.* **143,** 477 (1988).
10. Weyda, H., and Lechert, H., *Zeolites* **10,** 251 (1990).
11. Dzwigaj, D. S., Briend, M., Shikholesami, A., Peltre, M. J., and Barthomeuf, D., *Zeolites* **10,** 157 (1990).
12. Ojo, A. F., Dwyer, J., Dewing, J., O'Malley, P. J., and Nabhan, A., *J. Chem. Soc., Faraday Trans.* **88**(1), 105 (1992).
13. Bezouhanova, C., Kalvachev, Y., and Lechert, H., *J. Chem. Soc., Faraday Trans.* **87**(19), 3315 (1991).
14. Akolekar, D. B., "Sorption, Diffusion and Catalytic Reactions on Zeolites and Zeolite-like Materials." Ph.D. thesis, University of Poona, Poona, 1987.
15. Choudhary, V. R., Akolekar, D. B., Singh, A. P., and Sansare, S. D., *J. Catal.* **111,** 254 (1988).
16. Akolekar, D. B., and Kaliaguine, S., *Microporous Mater.* **2**(2), 137 (1994).
17. Akolekar, D. B., and Kaliaguine, S., *J. Chem. Soc., Faraday Trans.* **89**(22), 4141 (1993).
18. Ward, J. W., *in* "Zeolite Chemistry and Catalysis" (J. A. Rabo, Ed.) p. 118. ACS Monograph, Vol. 171, ACS, Washington DC, 1976.
19. Arlidge, E. Z., and Farmer, V. C., *J. Appl. Chem.* **13,** 17 (1963).
20. Tapp, N. J., and Milestone, N. B., *Zeolites* **10,** 105 (1990).
21. Moffat, J. B., Vetrivel, R., and Viswanathan, P., *J. Mol. Catal.* **30,** 171 (1985).
22. Choudhary, V. R., and Akolekar, D. B., *J. Catal.* **103,** 115 (1987).